Optics Letters

# Efficient wideband tunable radio frequency–optical conversion via triply resonant photonic molecules

Manuj Singh,[1,*] Xinchang Zhang,[1] Bohan Zhang,[1] Deniz Onural,[1] Hayk Gevorgyan,[1] Ruocheng Wang,[2] Vladimir M. Stojanović,[2] and Miloš A. Popović[1]

[1]Department of Electrical and Computer Engineering and Photonics Center, Boston University, Boston, Massachusetts 02215, USA
[2]Department of Electrical Engineering and Computer Sciences, University of California Berkeley, Berkeley, California 94709, USA
*manujks@bu.edu

Received 23 April 2024; revised 4 June 2024; accepted 13 June 2024; posted 14 June 2024; published 10 July 2024

**Electro-optic (EO) transduction of weak radio frequency (RF) and millimeter-wave signals, such as those received by an antenna, onto laser sidebands for processing in the optical domain requires efficient EO modulators. Microrings offer spatial density and efficiency advantages over Mach–Zehnder modulators (MZMs), but conventional single-ring modulators suffer a fundamental trade-off between resonantly enhanced conversion efficiency and the RF carrier frequency that it can accommodate. Dual-cavity "photonic molecule" modulators resolve this trade-off, allowing high efficiency independent of the RF carrier frequency by providing separate resonant supermodes to enhance the laser local oscillator (LO) and the narrowband RF-detuned sideband. However, the RF frequency is fixed at design time by geometry, with efficiency dropping quickly for RF carriers away from the design value. We propose a novel, to the best of our knowledge, triple-cavity configuration with an off-resonant middle ring acting as an effective tunable coupler between two active modulator cavities. This configuration provides wideband tunability of the target RF carrier while maintaining efficient sideband conversion. When the middle ring is passive (high $Q$), this configuration provides wide RF tunability with no efficiency penalty over the fixed dual-cavity case and could become an important building block for future RF/mm-wave photonic integrated circuits (PICs).** © 2024 Optica Publishing Group. All rights, including for text and data mining (TDM), Artificial Intelligence (AI) training, and similar technologies, are reserved.

https://doi.org/10.1364/OL.528080

**Introduction.** Photonic integrated circuits (PICs) could play an important role in the processing of radio frequency (RF) and millimeter-wave signals, including in phased-array antennas for 5G/6G+ wireless communication [1–3] and radar, in Earth sensing [4], and in optical clocks and RF frequency synthesizers. RF-to-optical (EO) transducers are critical elements for such circuits. If made efficient, compatible with scaling to large-scale circuits, compact enough to fit within the millimeter-wave phased-array antenna element spacing, and monolithically integrable with RF-CMOS circuits, such as low-noise amplifiers, they could enable a powerful new class of electronic–photonic integrated circuits for RF/mm-wave applications.

Traditional methods for electro-optic (EO) RF signal transduction rely on Mach–Zehnder modulators (MZMs). MZMs are large and present velocity-matching challenges that limit transduction bandwidth. Conventional microring modulators offer smaller footprint than MZMs, but present a trade-off between high conversion efficiency and high RF carrier frequency. The efficiency of resonant modulator designs scales with quality factor to mode volume ratio, Q/V. Designs based on matching the free spectral range (FSR) of an optical ring resonator [5,6] to the RF drive frequency have been explored to leverage the high $Q$ to enhance the EO interaction in the modulators. However, such designs show a trade-off between the FSR and mode volume restricting these devices to operate more efficiently at high (THz) RF carrier frequencies.

Dual-cavity modulators [7–9] break this trade-off, allow small mode volume while preserving high $Q$, and enable efficient RF–optical conversion over a range of practical RF carrier frequencies. But a limitation is that their matching of a fixed supermode (SM) splitting to the RF carrier maximizes efficiency at a single RF frequency fixed at design time.

Conceptually, this limitation can be circumvented using an adjustable cavity–cavity coupling (e.g., coupling gap) to produce a tunable SM splitting (Fig. 1), but a practical implementation is lacking. This method enables the highest RF-to-optical conversion efficiencies over a range of RF carrier frequencies through matching of the SM splittings with an arbitrary RF drive frequency. However, in scalable integrated photonics platforms, physically adjusting the ring-to-ring coupling gaps in real time is not practically realizable without introducing MEMS and added complexities. One solution for solid-state tuning of coupling strength is to use a Mach–Zehnder interferometer (MZI) [Fig. 2(a)] by thermally controlling the phase between its two arms [10]. However, such use of MZIs degrades the sideband generation efficiency because they can significantly enlarge the mode volume and deteriorate Q/V, add intrinsic loss due to the inclusion of strong 3-dB couplers which have parasitic loss, and exclude some of the resonator from the active area.

**Modeling.** We propose a practical implementation for a tunable-RF-frequency modulator using a triple-cavity configuration. A detuned middle cavity acts as a tunable coupling



Corrected 15 July 2024

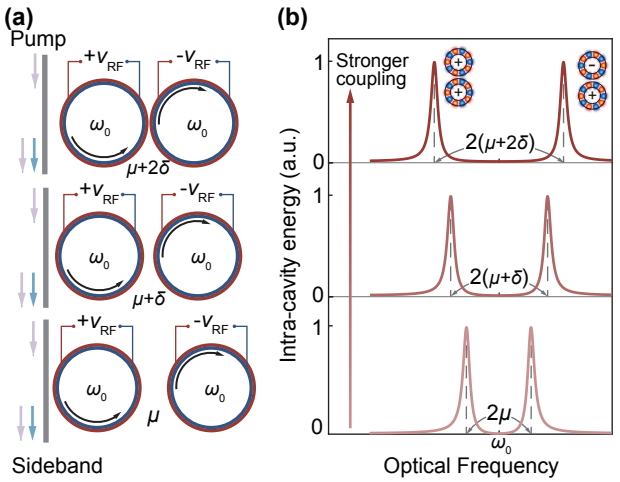


**Fig. 1.** (a) Dual-cavity modulators showing two coupled cavities that are driven anti-symmetrically and in-resonance. For illustration, three structures are shown with incremented coupling strength from $\mu$ to $\mu + 2\delta$ (bottom to top). The optical pump is assumed to excite the symmetric SM in each case (bottom to top). (b) Corresponding SM splittings resulting from the ring–ring coupling strengths in (a).

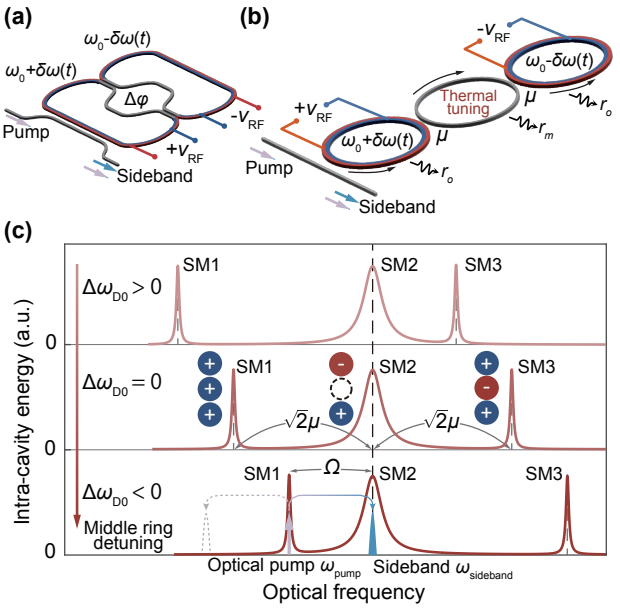


**Fig. 2.** (a) Dual-cavity modulators incorporating tunable MZI coupling to control SM resonance splitting. (b) Proposed triple-cavity modulators with middle ring resonance detuning $\Delta\omega_{D0}$. (c) Illustrations depict the effect of $\Delta\omega_{D0}$ on the SMs of the proposed triple-cavity modulators. SM 1, 2, and 3 resonances are shown from left to right in each inset.

between two active cavities [Fig. 2(b)] and produces a spectrum of three supermodes (SMs), SM1, SM2, and SM3 [Fig. 2(c)]. The two outer rings are driven in push–pull configuration. When we detune the middle ring by $\Delta\omega_{D0}>0$, SM 2's resonance frequency remains fixed, while the SM 1 and SM 3 frequencies blueshift together [Fig. 2(c)]. This allows the spacing between two of these SMs to match the tunable RF frequency $\Omega$ and achieve tunable single-sideband generation.

For the compound resonator to support optimum RF–optical conversion, the RF frequency should *match the spacing* of two optical SMs that have *substantial RF–optical–optical mode overlap*. Both are controlled by the detuning of the middle cavity and can be obtained from a temporal coupled-mode theory (T-CMT) model [Figs. 3(a) and 3(b)] [8,11]. We assume three rings (first with no bus waveguides) coupled serially by identical coupling coefficient $\mu$. The case of un-identical couplings due to fabrication errors causing coupling mismatch is shown in Supplement 1. In the absence of modulation and ring resonance detunings, we define $a_1$, $a_2$, and $a_3$ as energy amplitudes of the optical fields in individual micro-cavities that oscillate at resonance frequency $\omega_o$. The outer and middle cavities are assumed to have intrinsic decay rates $r_o$ and $r_m$, respectively. $\delta\omega(t)$ represents the instantaneous change in the resonance frequencies due to the push–pull modulation. Now, we include resonance detuning $\Delta\omega_{D0}$ of the middle ring such that the middle ring resonance $\omega_D$ becomes $\omega_D = \omega_0 + \Delta\omega_{D0}$. We write the CMT equations as

$$\frac{d}{dt}\bar{a} = j\bar{\bar{\omega}}\cdot\bar{a} - j\bar{\bar{\mu}}\cdot\bar{a} \tag{1}$$

where

$$\bar{a} = \begin{bmatrix} a_1 \\ a_2 \\ a_3 \end{bmatrix}, \quad \bar{\bar{\mu}} = \begin{bmatrix} 0 & \mu & 0 \\ \mu & 0 & \mu \\ 0 & \mu & 0 \end{bmatrix},$$

$$\bar{\bar{\omega}} = \begin{bmatrix} \omega_0 - \delta\omega(t) + jr_o & 0 & 0 \\ 0 & \omega_0 + jr_o + H & 0 \\ 0 & 0 & \omega_0 + \delta\omega(t) + jr_o. \end{bmatrix}$$

and $H = \Delta\omega_{D0} + j(r_m - r_o)$. Solving Eq. (1), the unmodulated ($\delta\omega = 0$) SM frequencies and normalized eigenvectors are

$$\begin{aligned} \omega_1 &= \omega_o + jr_o - T, & \bar{b}_1^T &= (\mu, T, \mu)\frac{1}{\sqrt{2\mu^2 + T^2}}; \\ \omega_2 &= \omega_o + jr_o, & \bar{b}_2^T &= \left(\frac{1}{\sqrt{2}}, 0, -\frac{1}{\sqrt{2}}\right); \\ \omega_3 &= \omega_o + jr_o + \frac{2\mu^2}{T}, & \bar{b}_3^T &= \left(\mu, -\frac{2\mu^2}{T}, \mu\right)\frac{-T}{\sqrt{2\mu^2 + T^2}\sqrt{2}\mu}, \end{aligned} \tag{2}$$

where $T \equiv \sqrt{(H/2)^2 + 2\mu^2} - H/2$ which represents total frequency splitting between the first and second SMs. $\omega_i$ and $\bar{b}_i$ represent the SM eigenfrequencies and corresponding normalized energy amplitudes which can be written as a function of normalized middle ring detuning $\Delta\omega_{D0}/\Omega_o$ for $i = 1, 2, 3$. Here $\Omega_o$ is the splitting when $\Delta\omega_{D0} = 0$ (and the carrier frequency of the RF drive signal for this nominal configuration). For the optimal design, assumed above, $\mu = \Omega_o/\sqrt{2}$.

**Impact of middle ring detuning $\Delta\omega_{D0}$ on triple-cavity modulator.** We plot the dependence of the eigen-mode field amplitudes and eigenfrequencies for the proposed triple-cavity configuration versus $\Delta\omega_{D0}/\Omega_o$ in Figs. 3(a) and 3(b), respectively. The energy distribution across cavities for SM 2 [Fig. 3(a), middle] and its eigenfrequency remain unchanged when middle ring detuning is applied [Fig. 3(b)]. When we detune the middle ring by a $\Delta\omega_{D0}>0$, the relative energy fraction inside the outer rings of SM 1 [Fig. 3(a), top] increases and the SM splitting between SM 2 and 1 decreases [Fig. 3(b)]. Conversely, the SM splitting between SM 2 and 3 increases [Fig. 3(b)], shifting more energy to the (unmodulated) middle ring [Fig. 3(a), bottom].

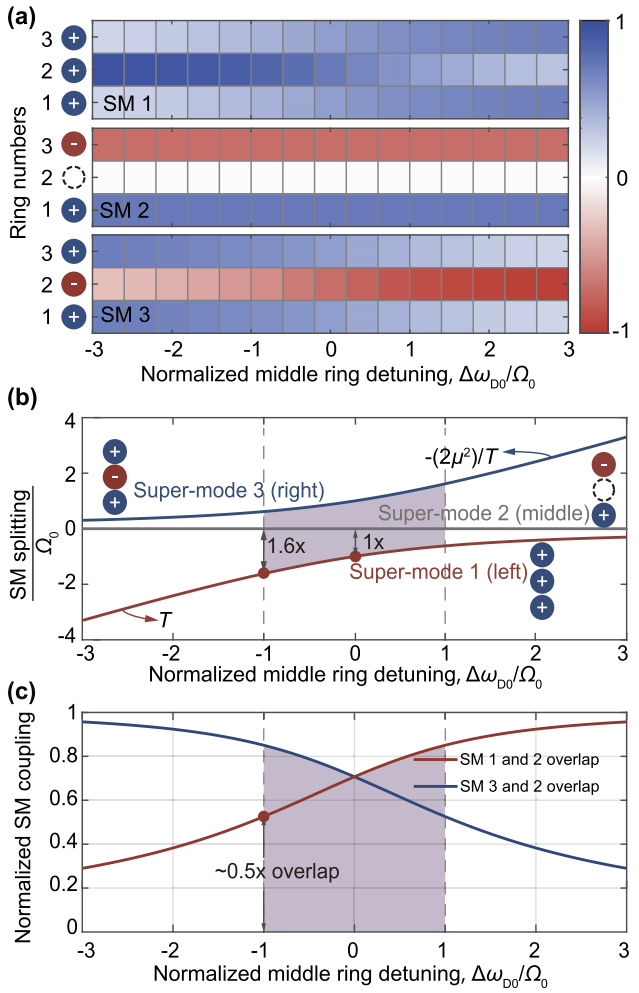


**Fig. 3.** (a) Distribution of cavity field amplitudes in each of the three SMs versus middle ring detuning $\Delta\omega_{D0}/\Omega_o$, (b) SM splitting, and (c) inter-SM coupling strength (proportional to conversion efficiency) relative to "ideal" dual-cavity configuration versus $\Delta\omega_{D0}/\Omega_o$. The SM 1–2 configuration drops below 50% of the maximum efficiency for $\Delta\omega_{D0} < -1$.

Excessive detuning $\Delta\omega_{D0}$ (to match mode splitting to the RF carrier) can eventually suppress the conversion efficiency by decoupling the cavities of the compound resonator, leading to a poor nonlinear mixing as captured in an RF–optical–optical overlap integral (with optical SMs). Figure 3(c) shows the normalized SM coupling strength, which is representative of the efficiency of sideband generation for cases when the laser pump is assumed to be driving SM 1 or 3, and the sideband is generated in SM 2. In that case, the SM coupling between the SMs 1 and 3 is zero. Detuning the middle ring by $\Delta\omega_{D0}<0$ increases the splitting between SM 1 and 2 [Fig. 3(b)] but decreases the coupling between them [Fig. 3(c)]. This represents one of the trade-offs of this approach. Tuning the SM splitting (and thus the RF drive frequency $\Omega$) below $\Omega_o$ improves the overlap, approaching ideal dual-cavity performance, while increasing the splitting reduces efficiency. Despite this, Figs. 3(b) and 3(c) show that the splitting can be 0 to 1.6 times $\Omega_o$ before the SM coupling (i.e., efficiency) is degraded to half, showing a wide range of operation. For Fig. 3(c), we calculate the SM coupling of the triple-cavity configuration based on the energy mode overlap analysis [5] when detuning the middle ring resonator (see Supplement 1). We normalize the SM coupling of the triple cavity to the SM overlap of an equivalent dual-cavity configuration formed by directly coupling the outer rings of the triple-cavity configuration to each other and removing the middle ring. The equivalent dual-cavity configuration has the same SM splitting as the splitting between SM 1 and 2 of the triple-cavity when $\Delta\omega_{D0} = 0$ (ideal case).

**Conversion efficiency.** We introduce coupling of the supermodes to input/output ports by adding an optical input coupled to SM 1 and assuming that the optical sideband is generated in SM 2. We apply a harmonic drive signal $\delta\omega(t) = \frac{\delta\omega_m}{2}\cos(\Omega t)$ where $\Omega$ is the arbitrary RF frequency and $\delta\omega_m$ is the peak-to-peak resonance shift. Following the same approach described in [8], we find the sideband conversion efficiency of triple-cavity modulators (see Supplement 1) when detuning $\Delta\omega_{D0}$ is applied to the middle cavity as

$$\left|\frac{\tilde{S}_{2-}}{\tilde{S}_{1+}}\right|^2 = \left|\frac{j2\sqrt{r_{e,m}r_{e,o}}\left(\frac{\delta\omega_m}{4}\frac{\sqrt{2}\mu}{\sqrt{2\mu^2+T^2}}\right)}{(r_o + r_{e,o} - \beta)(r_o + r_{e,m}) + \left(\frac{\delta\omega_m}{4}\frac{\sqrt{2}\mu}{\sqrt{2\mu^2+T^2}}\right)^2}\right|^2. \quad (3)$$

Here $\beta$ is the imaginary part of SM splitting $T$. $r_m$ and $r_o$ are the intrinsic decay rates (loss) of the middle and outer cavities, respectively. $r_{e,o}$ and $r_{e,m}$ are the external (outcoupling) decay rates for *the outer and middle SMs*, respectively. $\tilde{S}_{2-}$ and $\tilde{S}_{1+}$ are the wave amplitudes leaving SM 2 and exciting SM 1 in the bus waveguide, respectively.

**Tunable performance of the triple-cavity modulator.** Figure 4 shows the estimated efficiency and tunability of the triple-cavity configuration with middle ring detuning compared to dual-cavity modulators. Using Eq. (3), we compare the efficiency of a triple-cavity modulator across RF frequencies with the dual-cavity modulator in a silicon implementation [9]. A dual-cavity modulator has demonstrated a conversion efficiency of −11 dB at 24 GHz for a peak-to-peak resonance shift of 3.6 GHz driven with a peak-to-peak voltage drive of 4 V when biased at −1.5 V. The intrinsic $Q$ for the individual cavities was measured to be 70,000 (limited by doping). We assume a triple-cavity configuration formed out of the dual-cavity resonators possessing the same cavity parameters with two differences. First, the middle-to-edge SM splitting for the triple-cavity case is assumed to match the SM splitting of the dual-cavity case when no detuning is applied. Second, we assume critical coupling to SM 1 in the triple-cavity configuration and tune the pump to SM 1 while applying arbitrary RF drive frequency. Based on these assumptions, we project that the conversion efficiency ranges from −11.5 to −17.1 dB when we selectively detune the middle ring to allow SM matching of SMs 1 and 2 with a set of RF drive frequencies spanning two octaves, from 12 to 48 GHz (Fig. 4). Once SM splitting ($T/\Omega_o$) is set (in several configurations) by means of fixing the middle ring detuning $\Delta\omega_{D0}$, the conversion efficiency plots show a roll-off when the RF drive frequency deviates from the set SM splitting. This shows that the triple-cavity configuration allows tunable and efficient RF-to-optical conversion by selectively matching the SM splittings with arbitrary RF carrier $\Omega$ *in situ*, i.e., during device operation.

**Impact of middle ring *Q*.** A further insight comes from noting that the middle cavity for coupling control is not a modulator and can be made fully passive (high $Q$). With a high-$Q$ middle cavity, our model shows that the conversion efficiency of

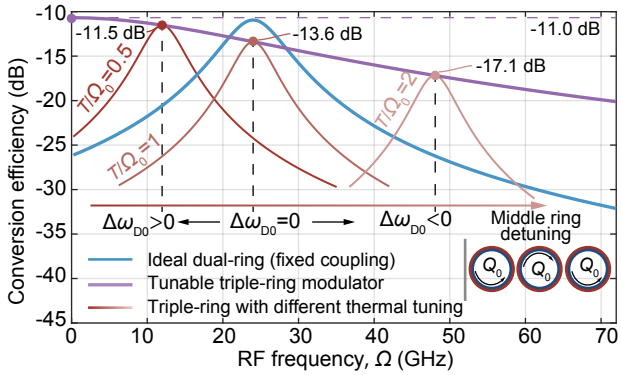


**Fig. 4.** Tunable modulation response of a triple-cavity configuration versus RF drive frequency Ω and compared with an ideal dual-cavity configuration [9] optimized for an RF drive frequency of 24 GHz. The three red Lorentzian plots are modulation responses of the triple-cavity when SM splitting $T/\Omega_o$ is fixed by three different middle-ring detuning configurations.

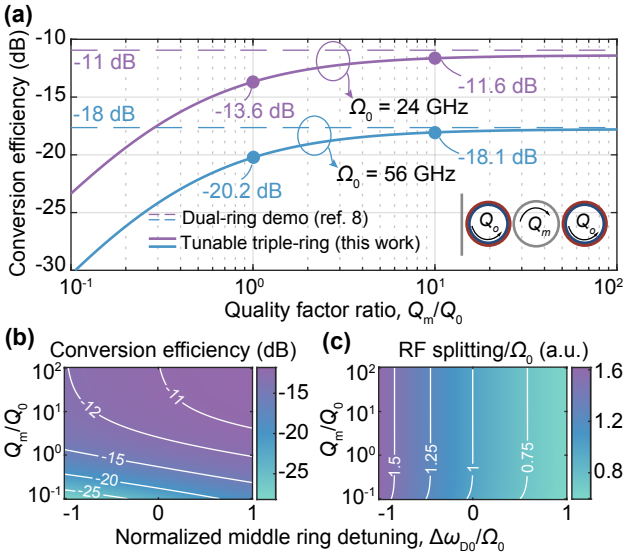


**Fig. 5.** (a) RF–optical conversion efficiency versus $Q_m/Q_o$ for two RF ($\Omega_o$) cases, (b) RF–optical conversion efficiency, and (c) RF splitting, $T/\Omega_o$, versus the thermooptic detuning of the middle ring, $\Delta\omega_{D0}/\Omega_o$, and middle ring loss Q, $Q_m/Q_o$.

the triple-cavity design can approach the ideal dual-cavity fixed design, producing a tunable RF design at no efficiency penalty (Fig. 5).

Using Eq. (3), the conversion efficiency as a function of the middle ring quality factor $Q_m$ normalized to the intrinsic quality factor $Q_o$ of the outer rings is shown in Fig. 5(a). No middle ring detuning is applied when the triple-cavity configuration is optimized to be driven either at 2 or 56 GHz in Fig. 5(a). For the two RF frequencies considered, the dual-ring configurations are different and optimized for the corresponding frequencies. As $Q_m/Q_o$ increases from 1 to 10, the estimated conversion efficiency improves from −13.6 to −11.6 dB approaching the dual-cavity conversion efficiency of −11 dB at 24 GHz. Similarly, when optimized for $\Omega_o = 56$ GHz, the estimated conversion efficiency increases from −20.2 to −18.1 dB when normalized middle ring $Q_m/Q_o$ increases from 1 to 10. Higher middle ring $Q$ allows better SM 1 and 3 Qs since considerable amounts of energy circulate within the middle cavity in SMs 1 and 3 when $\Delta\omega_{D0} = 0$. Thus, conversion efficiency improves when $Q_m > Q_0$. Finally, Fig. 5(b) shows the impact of incorporating a higher $Q$ middle ring such as $Q_m = 10Q_o$ also lowers the degradation of the conversion efficiency (from −10.8 to −12.4 dB) when the middle ring detuning $\Delta\omega_{D0}/\Omega_o$ is varied from +1 to −1 improving the tunability. This is significantly better conversion efficiency degradation as compared to the case when middle ring $Q_m = Q_o$ (from −11.9 to −15.8 dB). Figure 5(c) shows the corresponding SM splitting for various middle ring intrinsic $Q$s when we detune the middle ring resonance to achieve tunable RF-to-optical conversion.

**Conclusions.** Based on the presented concept and arguments, triply resonant modulators comprising two efficient modulation cavities and a third, detuned passive cavity in the middle to control the effective coupling of the former, could provide a versatile and efficient component for tunable RF-to-optical signal conversion. They can maintain high efficiency when tuned over one to two octave range of RF carrier frequency, with a small penalty in conversion efficiency over the ideal dual-cavity nontunable configuration. The penalty in the conversion efficiency is reduced by increasing the $Q$ of the middle ring producing a tunable RF design. They can approach efficiencies achievable in fixed-RF-frequency dual-cavity designs, addressing the issue of efficiency penalties from fabrication induced variation in the peak gain frequency of the modulator, a low-noise amplifier driving it, or other components in the system potentially rendering the latter impractical in many applications. The modulator could be a key building block of future on-chip millimeter-wave sensing, communication and photonic signal processing integrated systems, potentially realizable as silicon CMOS systems-on-chip.

**Funding.** National Science Foundation (2328946, FuSe).

**Disclosures.** Miloš A. Popović: Ayar Labs, Inc. (F,I,C), Vladimir M. Stojanović: Ayar Labs, Inc. (I,E).

**Data availability.** Data may be obtained from the authors upon reasonable request.

**Supplemental document.** See Supplement 1 for supporting content.

## REFERENCES

1. R. Wang, M. Singh, D. Onural, *et al.*, in *49th European Solid State Circuits Conference (ESSCIRC)* (2023).
2. M. Singh, R. Wang, D. Onural, *et al.*, in *49th European Conference on Optical Communications (ECOC)* (2023).
3. P. Sanjari and F. Aflatouni, Nat. Commun. **14**, 1414 (2023).
4. T. Pett, J. H. Lee, Y. Ehrlichman, *et al.*, *2018 International Topical Meeting on Microwave Photonics (MWP)* (2018).
5. L. D. Tzuang, M. Soltani, Y. H. D. Lee, *et al.*, Opt. Lett. **39**, 1799 (2014).
6. V. S. Ilchenko, A. A. Savchenkov, A. B. Matsko, *et al.*, J. Opt. Soc. Am. B **20**, 333 (2003).
7. M. T. Wade, X. Zeng, and M. A. Popović, Opt. Lett. **40**, 107 (2015).
8. H. Gevorgyan, A. Khilo, and M. A. Popovic, "Active-cavity photoni molecule optical data wavelength converter for silicon photonics platforms," arXiv (2020).
9. Y. Hu, M. Yu, D. Zhu, *et al.*, Nature **599**, 587 (2021).
10. A. H. Atabaki, B. Momeni, A. A. Eftekhar, *et al.*, Opt. Express **18**, 9447 (2010).
11. X. Zhang, M. Singh, D. Li, *et al.*, Opt. Lett. **49**, 3678 (2024).

128.197.28.178 (2024-10-11 17:23:35)